

## Determination of the complex microwave photoconductance of a single quantum dot

H. Qin,<sup>1</sup> F. Simmel,<sup>1,\*</sup> R. H. Blick,<sup>1</sup> J. P. Kotthaus,<sup>1</sup> W. Wegscheider,<sup>2,†</sup> and M. Bichler<sup>2</sup>

<sup>1</sup>Center for NanoScience and Sektion Physik, Ludwig-Maximilians-Universität, Geschwister-Scholl-Platz 1, 80539 München, Germany

<sup>2</sup>Walter-Schottky-Institut der Technischen Universität München, Am Coulombwall, 85748 München, Germany

(Received 13 January 2000; revised manuscript received 25 July 2000; published 2 January 2001)

A small quantum dot containing approximately 20 electrons is realized in a two-dimensional electron system of an  $\text{Al}_x\text{Ga}_{1-x}\text{As}/\text{GaAs}$  heterostructure. Conventional transport and microwave spectroscopy reveal the dot's electronic structure. By applying a coherently coupled two-source technique, we are able to determine the complex microwave-induced tunnel current. The amplitude of this photoconductance resolves photon-assisted tunneling (PAT) in the nonlinear regime through the ground state and an excited state as well. The out-of-phase component (susceptance) allows us to study charge relaxation within the quantum dot on a time scale comparable to the microwave beat period.

DOI: 10.1103/PhysRevB.63.035320

PACS number(s): 73.21.-b, 73.40.Gk, 73.50.Mx, 73.50.Pz

Spectroscopy on quantum dots is commonly performed either by nonlinear transport<sup>1,2</sup> or by microwave measurements.<sup>3-6</sup> Ordinary linear transport, i.e., under a small forward bias  $V_{ds}$  between source and drain contacts and without microwave irradiation, only involves quantum dot ground states. In the nonlinear case, by applying a finite bias across the “artificial atom,”<sup>7</sup> also excited quantum dot states can participate in transport. Alternatively, in the presence of a microwave field electrons can absorb or emit photons and thus reach excited quantum dot states otherwise not available in linear transport—a phenomenon known as photon-assisted tunneling (PAT).<sup>8</sup> In a combination of the two methods described, we use two coherently coupled microwave sources with a slight frequency offset and detect the complex photoconductance signal (microwave induced tunneling current) at the difference frequency. In this way, we are not limited by the broadening of the conductance resonances due to the finite bias and thus are able to resolve PAT in the nonlinear regime as well. Furthermore, the detected photoconductance contains the in-phase part (conductance) and out-of-phase part (susceptance). The variation of these two different responses indicates the different dynamics of the involved transport processes through the artificial atom.

For the observation of PAT through excited states the size of the quantum dot system is crucial: First, the dot has to be small enough to have a mean energy level spacing  $\bar{\Delta}$  large compared to the intrinsic or thermal broadening of the conductance resonances, i.e.,  $\Gamma, k_B T < \bar{\Delta} = 2\hbar^2/m^*r^2$ , where  $\Gamma$  denotes the intrinsic level broadening,  $T$  the temperature,  $r$  the radius of the dot, and  $m^* \approx 0.067m_e$  the effective electron mass. Second, the excited state must be attainable via absorption of one or a few photons, i.e.,  $hf \approx \bar{\Delta}$ , where  $f$  is the microwave frequency. In order to form such a small laterally confined quantum dot, patterned split gates are adopted to selectively deplete the two-dimensional electron system (2DES) of an  $\text{Al}_x\text{Ga}_{1-x}\text{As}/\text{GaAs}$  heterostructure. The split gates are fabricated on the surface of the heterostructure using electron beam lithography. A schematic drawing of the structure is shown in the inset of Fig. 1. The gate structure separates a small electronic island (with a lithographic radius of about 100 nm) from the 2DES via tunneling barriers. To

improve the shape of this island, a magnetic field of 1 T is applied perpendicularly to the plan of 2DES. The 2DES itself is located 50 nm below the surface of the heterostructure and has a carrier density of  $n_s \approx 2 \times 10^{11} \text{ cm}^{-2}$  and a low-temperature mobility of  $\mu \approx 8 \times 10^5 \text{ cm}^2/\text{Vs}$ .

In order to characterize the electronic structure of the artificial atom, at first standard direct current (dc) transport measurements without high-frequency irradiation are performed. The measurements are conducted in a dilution refrigerator at 140 mK bath temperature, which is higher than its possible minimum value of 20 mK. This is due to heat leakage through the coaxial lines used to couple the high-frequency radiation to our sample. In the tunneling regime at

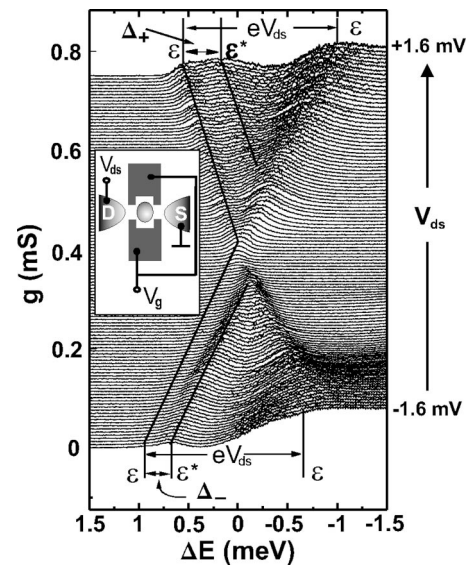


FIG. 1. Bias dependence of the quantum dot conductance in the vicinity of a single resonance: The drain-source bias is varied from  $V_{ds} = -1.6$  mV (bottom) to  $V_{ds} = +1.6$  mV (top) in 120 steps. The horizontal axis is the distance  $\Delta E = -e\alpha\Delta V_g$  from the zero-bias ground-state resonance (see text). The single resonance at  $V_{ds} = 0$  is split into two resonances separated by  $eV_{ds}$ . Additional resonances stem from excited states of the quantum dot  $\Delta_+$  and  $\Delta_-$  above the ground state, for positive and negative bias, respectively. The inset shows the gate structure that is used to define the quantum dot.

$V_{ds}=0$  the conductance of the quantum dot is normally zero due to Coulomb blockade (CB).<sup>2</sup> By tuning one of the gate voltages, however, the potential of the dot can be varied to align a discrete quantum dot state with the chemical potentials of the leads,<sup>9</sup> which results in a conductance resonance. The gate voltage range over which the CB is lifted can be increased by applying a finite bias across the quantum dot. Changing gate and bias voltage simultaneously therefore leads to a diamond-shaped conductance pattern in the  $V_{ds}$ - $V_g$  plane. The result is displayed in Fig. 1, where the differential conductance  $dI_{ds}/dV_{ds}$  in the vicinity of a resonance is shown as a function of forward bias  $V_{ds}$  and gate voltage  $V_g$ . For convenience, the gate voltage is rescaled to  $\Delta E = -e\alpha\Delta V_g$ , which is the energetic distance from the ground state resonance at  $V_{ds}=0$ . Here,  $\alpha = C_g/C$  is the ratio of gate capacitance  $C_g$  to the total capacitance  $C$  and is deduced from the slopes of the resonance lines in the  $V_{ds}$ - $V_g$  plane. The transformation to  $\Delta E$  allows for a direct extraction of excitation energies from the conductance plot.

From the zero-bias distance between adjacent conductance peaks the total capacitance of the quantum dot is determined to be  $C = 85$  aF. The quantum dot radius is thus estimated to be  $r = 70$  nm, i.e., the quantum dot contains only about 20 electrons. As expected, for nonzero bias the ground-state resonance (marked  $\epsilon$  in Fig. 1 for comparison with the excited state resonance  $\epsilon^*$ ) splits by  $eV_{ds}$ . For  $V_{ds} > 0$  an additional conductance resonance due to an excited state at  $\epsilon^*$  develops, which is  $\Delta_+ = (\epsilon^* - \epsilon) = 390$   $\mu\text{eV}$  above the ground state. Correspondingly, for  $V_{ds} < 0$  a resonance is detected at a distance  $\Delta_- = 280$   $\mu\text{eV}$  from the ground state. These excitation energies are in good agreement with the mean level spacing  $\bar{\Delta} \approx 465$   $\mu\text{eV}$  estimated from the dot radius. Hence, two different excited states take part in transport for  $V_{ds} < 0$  and  $V_{ds} > 0$ . Furthermore, as we can see from Fig. 1, the ground-state resonance for  $\Delta E > 0$  is almost suppressed for  $V_{ds} < 0$ , whereas the excited-state resonance for  $\Delta E > 0$  is much stronger. The origin of these ‘‘ $\Delta E > 0$ ’’ resonances are the alignment of the dot’s ground state or the excited state with the chemical potential of the drain reservoir. The strength of these resonances are related to the overlap between the wave function of the corresponding quantum dot state and the wave functions in the reservoirs. Hence, the variation in conductance indicates that the coupling of the ground state to the drain reservoir is much smaller than that of the excited state. This phenomenon was also observed in Ref. 1. In our case, we find that the coupling of the excited state to the reservoirs is about 5.3 times the coupling of the ground state.

Two different techniques are applied to study the transport properties under microwave irradiation. For low forward bias  $V_{ds} \approx 0$ , the direct current through the dot is measured using a single microwave source. Alternatively, we employ two phase-locked microwave sources which are slightly offset in frequency. This second technique allows to detect photon-induced transport also in the nonlinear regime  $|V_{ds}| > 0$ . Furthermore, the relative phase of the photon-induced current with respect to the incoming microwave beat can be determined.

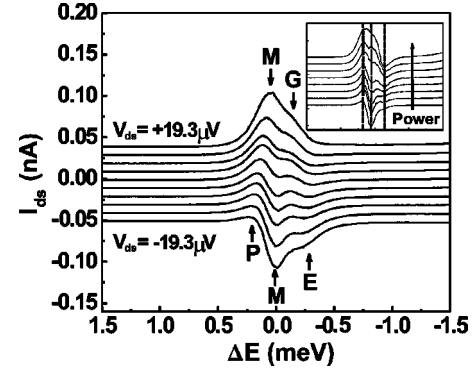


FIG. 2. Direct current through the quantum dot for small bias values under irradiation with microwaves of frequency  $f = 36.16$  GHz. Next to the main ground-state resonance ( $M$ ) additional features ( $G, P, E$ ) appear that can be ascribed to photon-assisted tunneling through the ground state, photon-induced pumping, and tunneling through an excited state (see text). In the inset the power dependence of these features is shown for  $V_{ds} = -5.1$   $\mu\text{V}$ . The output power of the microwave source is increased from bottom to top in steps of 0.5 dBm.

Results obtained with the first technique are shown in Fig. 2, where the current through the quantum dot for small bias ranging from  $-19.3$   $\mu\text{V}$  to  $+19.3$   $\mu\text{V}$  is displayed under microwave irradiation at frequency  $f = 36.16$  GHz. To this end, millimeter waves with frequency 18.08 GHz are generated by a microwave synthesizer (HP 87311A), then frequency-doubled (MITEQ MX 2V260400) and filtered using a band pass filter (QUINSTAR QFA-3715-BA) with center frequency at 32 GHz. The microwave signal is coupled into the cryostat using coaxial lines and irradiated onto the sample using an antenna formed out of a conducting loop. The coupling proved to be best at the chosen frequency 36.16 GHz. For small positive bias the original main peak from the ground-state resonance ( $M$ ) as well as a sideband ( $G$ ) in a distance  $hf \approx 0.15$  meV are detected. This sideband in the current signal is due to PAT through the ground state. Quite differently, for negative bias additional features in the current signal are induced by the microwaves. These features can be attributed to photon-induced pumping ( $P$ ) and resonant tunneling through an excited quantum dot state ( $E$ ). The processes involved are schematically depicted in Fig. 3: At low positive bias only the ground-state transition Fig. 3(a) occurs. As found in the preceding paragraphs, the first excited state for this bias direction is too far above the ground state to be accessible by a one- or two-photon process. The other possible photon-induced ground state transition ( $\Delta E > 0$ ) shown in Fig. 3(b) is not detected in the low-bias current signal. However, it is resolved for larger bias values applying the two-source detection scheme (see below). For negative bias  $V_{ds} < 0$  the excited state at  $\epsilon^* = \epsilon + \Delta_-$  can participate in transport when the ground state is depopulated by a two-photon absorption process [Fig. 3(c)] ( $2hf \geq \Delta_-$ ), a process analogous to photoionization.<sup>3</sup> Normally, this process has a much smaller probability than the one- and two-photon PAT processes. In our case, however, since the coupling of the excited state to the reservoirs is more than four times stronger than the coupling of the ground state, this

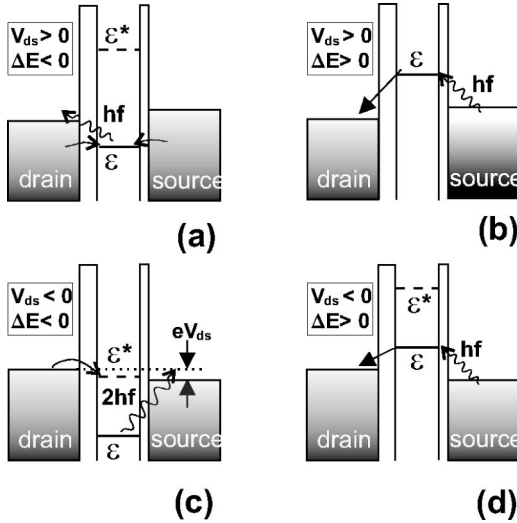


FIG. 3. Schematic representation of the photon-induced processes involved in Figs. 2, 5, and 6: In the case of positive bias (a, b), only photon-assisted tunneling through the ground state is possible. For  $V_{ds} < 0$ , the excited state  $\epsilon^*$  is approximately two photon energies above the ground state and can be accessed by absorption of two photons (c). Furthermore, due to the asymmetry in microwave absorption across the tunneling barriers, a pumping current can occur (d) for  $V_{ds} < 0$  (see text).

process might turn out to be comparable to the pure two-photon PAT in amplitude. This will be discussed in further detail below. Furthermore, a pumping current flows opposite to the bias direction for  $\Delta E > 0$ , where the ground state is  $hf$  above the chemical potentials in the source reservoir [Fig. 3(d)]. This only happens when the microwave absorption across the right tunnel barrier is larger than that of the left tunneling barrier. In this case, the ground state  $\epsilon$  is permanently populated with electrons from the source contact which then partly decays into the drain region. From the power dependence (see below), we confirm that this pumping current results from PAT.

Photon-induced features similar to our results have been reported before<sup>5</sup> and explained theoretically using, e.g., non-equilibrium Green-function techniques.<sup>10,11</sup> However, to ensure that the observed features are not adiabatic effects of the microwave irradiation (e.g., rectification effects<sup>12</sup>) commonly both their frequency and power dependence are determined. The inset of Fig. 2 shows the power dependence of the photon-induced features for  $V_{ds} = -5.1 \mu\text{V}$ . The output power of the microwave synthesizers is changed in steps of 0.5 dBm from trace to trace. Over this wide power range the microwave-induced features do not change in position showing that they are indeed induced by single photons. We find that the observed dependence of peak heights on microwave power roughly agrees with the Bessel function behavior: The tunneling current induced by absorbing/emitting  $n$  photons is proportional to  $J_n^2(x)$ , where  $x = eV_{ac}/hf$  and  $V_{ac}$  is the microwave amplitude across the tunnel barriers. This behavior was theoretically derived in Ref. 8 and was experimentally observed in Refs. 5 and 6. For even higher microwave powers the PAT-like features considerably broaden due to heating effects until they are finally completely washed out. Due

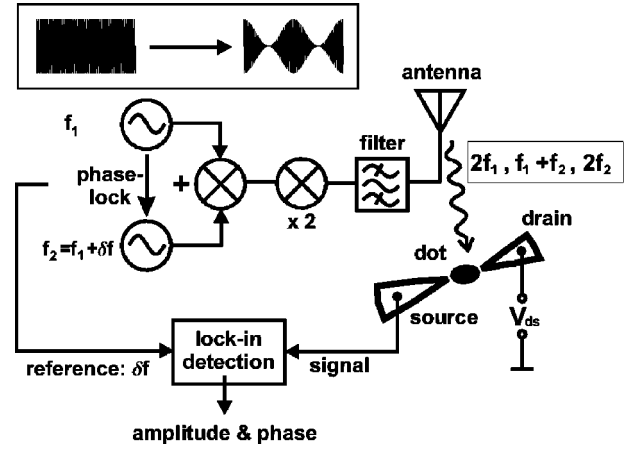


FIG. 4. Experimental setup for the two-source measurement: Two millimeter waves with a slight frequency offset generated by two phase-locked microwave synthesizers ( $f_1 = 18.08 \text{ GHz}$  and  $\delta f = 2.1 \text{ kHz}$ ) are added, doubled and filtered. The resulting modulated signal is irradiated on the quantum dot by means of an antenna. With a lock-in amplifier both the amplitude and the phase of the photoconductance are detected at the modulation frequency  $\delta f$ . In the inset the microwave signal before and after modulation is schematically depicted.

to the limited bandwidth of our high-frequency setup, we are not able to study the frequency dependence to identify the photon-induced peaks. Studying the power dependence only is not sufficient to reveal the origin of peak  $E$ . By determining the complex photoconductance, however, we will show that the out-of-phase component indicates some aspects of the origin (see below).

A more subtle spectroscopic tool applied in this work is the two-source setup displayed in Fig. 4: Two microwave synthesizers are phase-locked and tuned to slightly different frequencies  $f_1 = 18.08 \text{ GHz}$  and  $f_2 = 18.08 \text{ GHz} + \delta f$  with  $\delta f = 2.1 \text{ kHz}$ . The two signals are added, frequency-doubled and filtered with a band pass as described before. Due to the band pass only microwaves with frequencies  $2f_1$ ,  $f_1 + f_2$ , and  $2f_2$  are irradiated upon the quantum dot. As these frequency components have a rigid phase relation, their superposition leads to a modulated microwave signal with modulation frequency  $\delta f$  (see upper inset of Fig. 4). We have thus produced a flux of photons with energy  $\approx 2hf_1 = 0.15 \text{ meV}$  whose intensity varies periodically in time with frequency 2.1 kHz. Electronic transport induced by these photons can be detected with a lock-in amplifier at the frequency of the microwave beat. Thus, the detected signal is solely due to the irradiation and contains no dc contribution. It is therefore possible to observe PAT even in the nonlinear regime, where the broadening of the ordinary conductance resonances normally masks the photon-induced features. Another advantage of this technique is the possibility of heterodyne detection which allows for determination of both the amplitude and relative phase of the signal.<sup>13</sup> This is not possible using a single microwave source and a simple modulation technique with a p-i-n diode.

With the lock-in amplifier the in-phase and out-of-phase photoconductance signals  $\gamma_0$  and  $\gamma_{\pi/2}$  with respect to the

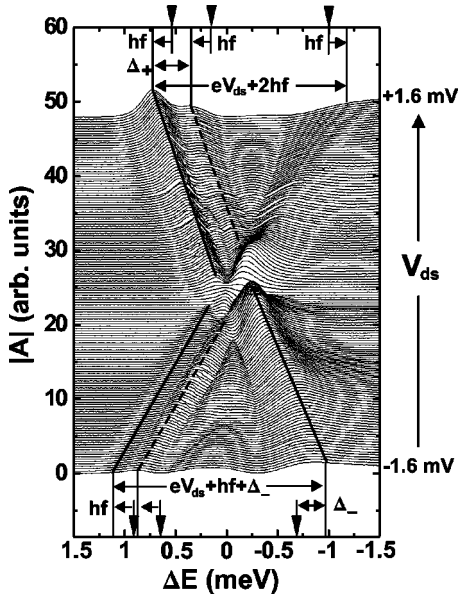


FIG. 5. Amplitude  $|A|$  of the photoconductance measurement obtained with the two-source setup of Fig. 4. The drain-source bias is varied as in Fig. 1. The position of the resonances found in the dc measurement of Fig. 1 are indicated with triangles. With respect to the dc resonances, most photoconductance resonances are shifted by the photon energy  $hf$ , as can be expected for photon-assisted processes. The resonance for  $V_{ds} < 0$  and  $\Delta E < 0$ , however, is shifted by  $\Delta_-$ , indicating two-photon PAT through a ground state and the resulting tunneling through an excited state as sketched in Fig. 3(c).

reference are measured. From these we obtain the total photoconductance amplitude  $|A| = \sqrt{\gamma_0^2 + \gamma_{\pi/2}^2}$  and the relative phase  $\Phi$ , which equals  $\arctan(\gamma_{\pi/2}/\gamma_0)$  for  $\gamma_0 \geq 0$  and  $\pi + \arctan(\gamma_{\pi/2}/\gamma_0)$  for  $\gamma_0 < 0$ , respectively. In Fig. 5 the photoconductance amplitude at  $f = 2f_1 = 36.16$  GHz and  $\delta f = 2.1$  kHz is displayed for the same parameter region as the dc measurement shown in Fig. 1. With respect to Fig. 1, for  $V_{ds} > 0$  the conductance window is enlarged by  $2hf$ . The resonances are each shifted by the photon energy  $hf$ , which can readily be explained by photon-assisted tunneling processes as in Figs. 3(a) and 3(b). This is also the case for the  $\Delta E > 0$  conductance resonances for negative bias. However, the resonance for  $\Delta E < 0$  and small negative bias is clearly shifted by  $\Delta_-$ , thus enlarging the conductance window to  $eV_{ds} + hf + \Delta_-$ . The process involved is taken as the finite bias version of the transition depicted in Fig. 3(c): An electron leaves the quantum dot's ground state for the source reservoir via absorption of two photons. Now, electrons can either refill the ground state or tunnel through the excited state as long as the ground state is depopulated. Transport through the excited state stops when an electron decays to the ground state, or an electron enters the quantum dot's ground state from the leads. With  $\Delta E < 0$  and larger negative bias, the photoconductance peak is apparently broadened. The broadening is partly due to other tunneling processes possible at large bias, e.g., one-photon PAT through the ground state. In fact, even at small negative bias there is small tunneling current in between the peaks  $M$  and  $E$ , which

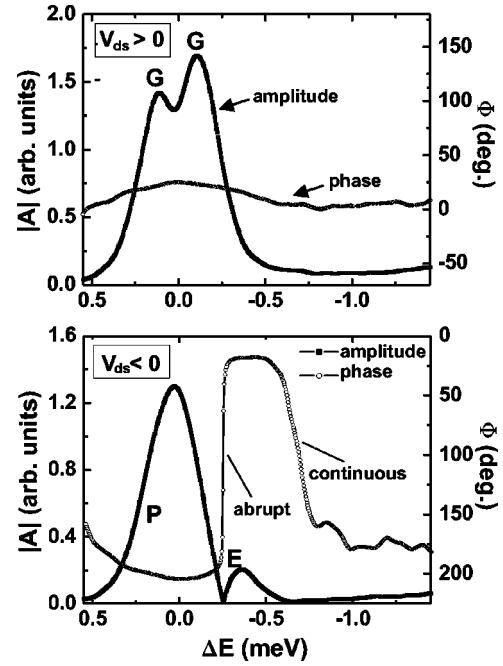


FIG. 6. Phase and amplitude of the photoconductance signal for  $V_{ds} = +10 \mu\text{V}$  (top) and  $V_{ds} = -30 \mu\text{V}$  (bottom). For positive bias, photon-assisted tunneling through the ground state ( $G$ ) is observed, as schematically depicted in Figs. 3(a) and 3(b). The phase signal remains constant on either side of the resonances. For negative bias, pumping ( $P$ ) and tunneling through an excited state ( $E$ ) are induced [cf. Figs. 3(d) and 3(c)]. Vanishing of the amplitude signal between  $P$  and  $E$  is accompanied by a trivial jump of  $\pi$  in the phase signal. Finally, for more negative values of  $\Delta E$  the phase signal continuously falls back to its original value.

is most probably the one-photon PAT. In our case, the tunneling process for  $\Delta E < 0$  and negative bias is more intricate than the ideal PAT.

In Fig. 6, phase traces as well as their respective amplitude signals are displayed for small positive and negative bias ( $V_{ds} = +10 \mu\text{V}$  and  $V_{ds} = -30 \mu\text{V}$ , respectively), corresponding to the central region of Fig. 5. For  $V_{ds} > 0$  the phase signal remains approximately constant at  $\Phi = 0$  which means that the out-of-phase photoconductance  $\gamma_{\pi/2}$  is equal to zero. The response of the quantum dot to the microwaves is similar for both of the tunneling processes ( $G$ ). In fact, the two peaks  $G$  in the amplitude signal stem from ground-state resonances as depicted in Figs. 3(a) and 3(b). The situation is considerably different for  $V_{ds} < 0$ , where a strong pumping signal ( $P$ ) is observed that is caused by a process as shown in Fig. 3(d). At the position where the photocurrent changes its direction, the amplitude drops to zero and the phase changes trivially by  $\pi$  (this corresponds to crossing zero in the  $\gamma_0 - \gamma_{\pi/2}$  plane). The second peak ( $E$ ) stems from the photon-induced tunneling through the excited state as shown in Fig. 3(c). Moving away from this second resonance to more negative  $\Delta E$ , the phase continuously returns to its original value.

This continuous phase change shows that this transport process results in a finite out-of-phase signal  $\gamma_{\pi/2}$ . In contrast to the other transport scenarios described above (only the ground state is involved), photon-induced tunneling

through the excited state is not a purely conductive transport process but also has capacitive and inductive contributions. This behavior is due to the complicated charging dynamics of the quantum dot for this particular process. The processes involved are PAT from the ground state to the source reservoir, resonant tunneling through the excited state, recharging of the ground state by the drain reservoir, and relaxation from the excited state to the ground state. All these processes have different time constants that additionally depend on the gate voltage (i.e.,  $\Delta E$ ). The interplay of these processes results in the observed phase lag. Thus one has a method at hand to determine the admittance of a mesoscopic system<sup>14–16</sup> in the PAT regime that is related to the average relaxation time of the system. In the current setup, for  $V_{ds} < 0$  the ground-state broadening, due to the coupling to the drain reservoir, is about 400 MHz, while the level broadening from the coupling to the source reservoir is around 2 GHz. The broadening of the excited-state coupling to the reservoirs is found to be of the same width of 2 GHz. Hence, the bare tunneling time through the ground state, excluding other time constants, would be less than 2.5 ns. However, the inverse modulation frequency  $1/\delta f \approx 500 \mu\text{s}$ , which is the time separation between two microwave beat minima, is much larger than the tunneling time. In the few-electron limit, this indicates that it takes the electron a much longer time to relax within the dot than to tunnel through the barriers. An extension of the measurements to modulation frequencies on the order of 10–100 MHz, corresponding to a time scale of 10–100 ns, would therefore be desirable. With a shorter microwave beat period we will be able to probe

both the fast tunneling event and the slow relaxation process. We conclude that with the frequency  $f$  the photon energy  $hf$  for the photon-induced process can be adjusted, whereas the modulation frequency  $\delta f$  determines the time scale on which the electronic dynamics of the quantum dot is probed.

In summary, we have presented complex photoconductance measurements in the nonlinear transport regime of a few-electron quantum dot using phase-locked microwave sources. The electronic structure of the dot is first characterized by conventional conductance measurements without microwave radiation. Photon-assisted tunneling through the ground state as well as through excited states of the system is observed. The two-source method allows to perform PAT measurements even in the nonlinear transport regime. Most importantly, the relative phase of the photocurrent with respect to the incoming microwave beat signal can be obtained from the two-source measurement. This phase is related to the susceptance of the quantum dot at very high frequencies. Nontrivial values for this quantity can be attributed to the long charge relaxation times in the quantum dot. In future work this can be exploited for an accurate determination of the relaxation times of excited quantum dot states.

We thank Q. F. Sun, A. W. Holleitner, and S. Manus for helpful discussions. This work was funded in part by the Deutsche Forschungsgemeinschaft within project SFB 348 and the Defense Advanced Research Projects Agency (DARPA) Ultrafast Electronics Program. H.Q. gratefully acknowledges support by the Volkswagen Stiftung.

\*Present address: Bell Laboratories, Lucent Technologies, 600 Mountain Ave, Murray Hill, NJ 07974.

<sup>†</sup>New address: Universität Regensburg, Universitätsstr. 31, D-93040 Regensburg, Germany.

<sup>1</sup>J. Weis, R.J. Haug, K. von Klitzing, and K. Ploog, Phys. Rev. Lett. **71**, 4019 (1993).

<sup>2</sup>L. P. Kouwenhoven, C. M. Marcus, P. L. McEuen, S. Tarucha, R. M. Westervelt, and N. S. Wingreen, in *Mesoscopic Electron Transport*, edited by L. L. Sohn, L. P. Kouwenhoven, and G. Schön (Kluwer Dordrecht, Netherlands, 1997), Series E, Vol. 345, pp. 105–214, see also references therein.

<sup>3</sup>L.P. Kouwenhoven, S. Jauhar, J. Orenstein, P.L. McEuen, Y. Nagamune, J. Motohisa, and H. Sakaki, Phys. Rev. Lett. **73**, 3443 (1994).

<sup>4</sup>R.H. Blick, R.J. Haug, D.W. van der Weide, K. von Klitzing, and K. Eberl, Appl. Phys. Lett. **67**, 3924 (1995).

<sup>5</sup>T.H. Oosterkamp, L.P. Kouwenhoven, A.E.A. Koolen, N.C. van der Vaart, and C.J.P.M. Harmans, Phys. Rev. Lett. **78**, 1536 (1997).

<sup>6</sup>T.H. Oosterkamp, T. Fujisawa, W.G. van der Wiel, K. Ishibashi, R.V. Hijman, S. Tarucha, and L.P. Kouwenhoven, Nature

(London) **395**, 873 (1998).

<sup>7</sup>R.C. Ashoori, Nature (London) **379**, 413 (1996).

<sup>8</sup>P.K. Tien and J.P. Gordon, Phys. Rev. **129**, 647 (1963).

<sup>9</sup>For simplicity, we adopt a rather sloppy formulation here. In fact, it is the discrete chemical potential  $E(N+1) - E(N)$  of the quantum dot associated with the ground-state transition  $N+1 \leftrightarrow N$  that is aligned with the chemical potential of the leads.

<sup>10</sup>C.A. Stafford and Ned S. Wingreen, Phys. Rev. Lett. **76**, 1916 (1996).

<sup>11</sup>Q. Sun, J. Wan, and T. Lin, Phys. Rev. B **58**, 13 007 (1998).

<sup>12</sup>J. Weis, R.J. Haug, K. von Klitzing, and K. Eberl, Semicond. Sci. Technol. **10**, 877 (1995).

<sup>13</sup>R.H. Blick, D.W. van der Weide, R.J. Haug, and K. Eberl, Phys. Rev. Lett. **81**, 689 (1998).

<sup>14</sup>Y. Fu and S.C. Dudley, Phys. Rev. Lett. **70**, 65 (1993).

<sup>15</sup>M. Büttiker, A. Prêtre, and H. Thomas, Phys. Rev. Lett. **70**, 4114 (1993).

<sup>16</sup>M. Büttiker, A. Prêtre, and H. Thomas, Phys. Rev. Lett. **71**, 465 (1993).